



HAL
open science

Sum-Frequency Generation at Molecule-Nanostructure Interfaces from Diagrammatic Theory of Nonlinear Optics

Thomas Noblet, Bertrand Busson

► **To cite this version:**

Thomas Noblet, Bertrand Busson. Sum-Frequency Generation at Molecule-Nanostructure Interfaces from Diagrammatic Theory of Nonlinear Optics. *Physical Review B*, 2022, 105 (20), pp.205420. 10.1103/PhysRevB.105.205420 . hal-03662629

HAL Id: hal-03662629

<https://hal.science/hal-03662629>

Submitted on 9 May 2022

HAL is a multi-disciplinary open access archive for the deposit and dissemination of scientific research documents, whether they are published or not. The documents may come from teaching and research institutions in France or abroad, or from public or private research centers.

L'archive ouverte pluridisciplinaire **HAL**, est destinée au dépôt et à la diffusion de documents scientifiques de niveau recherche, publiés ou non, émanant des établissements d'enseignement et de recherche français ou étrangers, des laboratoires publics ou privés.

Sum-Frequency Generation at Molecule-Nanostructure Interfaces from Diagrammatic Theory of Nonlinear Optics

T. Noblet¹ and B. Busson²

¹*GRASP-Biophotonics, CESAM, University of Liege,
Institute of Physics, Allée du 6 août 17, 4000 Liège, Belgium.*

²*Université Paris-Saclay, CNRS, Institut de Chimie
Physique, UMR 8000, 91405 Orsay, France.*

(Dated: May 9, 2022)

Abstract

We apply the loop diagrammatic method for linear and nonlinear optics to the calculation of the sum-frequency response of a molecule-nanostructure composite system. The presence of the nanostructure modifies the molecular response through dipolar energy exchange, and the molecular hyperpolarizability is factorized by nanostructure response functions of increasing orders. We provide a general method to transform these functions into products of first-order nanostructure polarizabilities, accounting for enhancements of the molecular response by coupling to plasmonic or excitonic resonances. Especially, we show how the diagrams may be directly read to determine the response functions and their factorization without explicit calculation. The methodology provides a frame for various applications to other systems, interactions and nonlinear optical processes.

I. INTRODUCTION

Within nonlinear optics, the second-order Sum-Frequency Generation (SFG) process has a variety of applications for the *in situ* analysis of molecular/inorganic interfaces [1–10], often composed of several subsystems. Despite the numerous articles reporting SFG data acquisition and analysis, the literature still lacks a general theory for such composite systems. Most of the times, SFG response is indeed split between molecules and substrate, then summed up to simulate experimental spectra [11, 12]. However, in recent years, the SFG response of complex systems has been experimentally determined, for which the SFG activity is shared between two interacting partners. The *ad hoc* models developed to account for such mechanisms do not share any common theoretical foundation [9, 13–20]. In order to fill this gap, we have established in a previous paper [21] a general formalism to represent elementary linear and nonlinear optical response functions by loop diagrams connected to the incoming (i.e. visible and infrared) and generated (i.e. SFG) photons by light-matter vertices. When the system giving birth to the optical process is composed of several subunits (e.g. molecules, substrate, nano-objects), this diagrammatic representation is very well suited to accounting for the interactions between the subsystems. Representing each subsystem by its own loop and defining their mutual interaction hamiltonian, it becomes possible to draw all the allowed diagrams involving new matter-matter vertices and to calculate them by following twelve Feynman rules [21] (recalled in Ref. [22], section 1.4). These apply to response functions expressed in terms of fermion propagators $\tilde{G}(i\omega)$ with imaginary (i.e. Matsubara) frequency

arguments [23, 24], allowing straightforward integration using the residue theorem before turning back to real frequencies.

In this Letter, we apply this new method to the popular case of molecule-nanostructure bipartite systems and demonstrate that this universal formalism allows to systematically recover the published *ad hoc* models and results of the literature. In this way, we show how to calculate the various relevant diagrams accounting for the modification of a molecular SFG response in the presence of any nano-object, and thus provide future users with useful and practical procedures to model their own bipartite systems. Furthermore, we prove that it is possible to express the second-order response functions, β , of the bipartite systems by simply reading the diagrams (here made of two loops) and to factorize them by elementary response functions, α (i.e. linear polarizabilities).

SFG is often exploited to perform vibrational spectroscopy, wherein the system, enlightened by two laser beams at frequencies ω_1 (e.g. visible) and ω_2 (e.g. infrared), generates a third one at frequency $\omega_3 = \omega_1 + \omega_2$. When surface-enhanced, vibrational spectroscopies like SFG and Raman facilitate the detection of molecular species. For surface-enhanced SFG, molecules interact with nanostructured metallic or semiconductor substrates, whose electronic properties amplify the optical response of the surrounding species. It is hard a task to model or predict the amplitude of such an amplification since it depends on the optoelectronic response of the substrate. The resulting second-order hyperpolarizability is often described by (see [21], Appendix C):

$$\beta_{ijk}(\omega_1, \omega_2) = \frac{1}{\hbar} \sum_v \frac{A_{ijk}^{(v)}(\omega_1, \omega_2)}{\omega_2 - \omega_v + i\Gamma_v}, \quad (1)$$

wherein the vibration amplitude $A_{ijk}^{(v)}(\omega_1, \omega_2)$ of each vibration mode $|v\rangle$ depends on the interactions between the molecules and the substrate. Henceforth, experimenters have to consider these vibration amplitudes as fitting parameters. In the following, we show how they can be analytically computed thanks to 2-loop diagrams.

II. DIAGRAMMATIC THEORY OF THE MOLECULE-NANOSTRUCTURE SYSTEMS

We consider a system composed of a nanostructure (e.g. nanoparticle, quantum dot), represented by one (upper) loop on the diagrams, with quantum states labeled by integers

m, n, q, r, s, t (associated to creation/annihilation operators c_m^\dagger, c_m, \dots), and a molecule, whose states are labeled by a, b and c (associated to creation/annihilation operators d_a^\dagger, d_a, \dots), described by a second (lower) loop. Each loop may interact with light at frequencies ω_1, ω_2 or ω_3 through a dipolar hamiltonian. We assume that the molecule and the nanostructure interact and may exchange energy through dipolar coupling, as driven by the hamiltonian [25]:

$$\begin{aligned}\mathcal{H}_{\text{int}} &= \boldsymbol{\mu} \cdot \mathbf{W}(\omega, \mathbf{R}) \mathbf{p} \\ &= \sum_{m,n,a,b} \sum_{h,l} W_{lh}(\omega, \mathbf{R}) \mu_{ab}^l p_{mn}^h c_m^\dagger d_a^\dagger c_n d_b,\end{aligned}\quad (2)$$

where $\mathbf{p} = (p^h)$ and $\boldsymbol{\mu} = (\mu^l)$ are the dipole moments of the nanoparticle and the molecule, respectively. This interaction process, associated to the coupling constant $\sum_{h,l} W_{lh}(\omega, \mathbf{R}) \mu_{ab}^l p_{mn}^h$, is in principle represented on the diagrams by a 4-particle vertex [21]. This interaction vertex is equivalently and conveniently represented by the exchange of a virtual boson (here, a virtual photon) from one loop to the other through two 3-particle vertices. Within this representation, the Feynman rules governing the vertices directly apply, with coupling constants μ_{ab}^l and p_{mn}^h , while $W_{lh}(\omega, \mathbf{R})$ represents the propagator (or the Green's function) of the virtual photon. According to electrodynamics [25], the coupling matrix is given by:

$$\begin{aligned}W_{lh}(\omega, \mathbf{R}) &= \frac{e^{i\omega|\mathbf{R}|/c}}{4\pi\epsilon_0|\mathbf{R}|^3} \left[(\delta_{lh} - 3\hat{R}_l\hat{R}_h) \left(1 - i\frac{\omega|\mathbf{R}|}{c} \right) \right. \\ &\quad \left. - (\delta_{lh} - \hat{R}_l\hat{R}_h) \left(\frac{\omega|\mathbf{R}|}{c} \right)^2 \right],\end{aligned}\quad (3)$$

where ω is the frequency of the exchanged virtual boson, \mathbf{R} the relative position of the nanostructure and the molecule, and $\hat{\mathbf{R}} = \mathbf{R}/|\mathbf{R}|$. When $\omega = 0$ (or $\omega|\mathbf{R}|/c \ll 1$), we retrieve the static case:

$$W_{lh}(0, \mathbf{R}) = \frac{\delta_{lh} - 3\hat{R}_l\hat{R}_h}{4\pi\epsilon_0|\mathbf{R}|^3}.\quad (4)$$

In the following, we drop the \mathbf{R} -dependence of matrix \mathbf{W} for clarity.

For this system, the full list of 2-loop diagrams describing the SFG process has been established [21]. Among these diagrams, only 48 encompass a molecular SFG response, and we therefore focus on these (Figures 1, 2 and 3) to compute the second-order response function $\beta_{ijk}(\omega_1, \omega_2)$ of the molecule under the influence of the nanostructure. They are grouped into four families defined by their number $V \in \{0; 1; 2; 3\}$ of virtual bosons. In

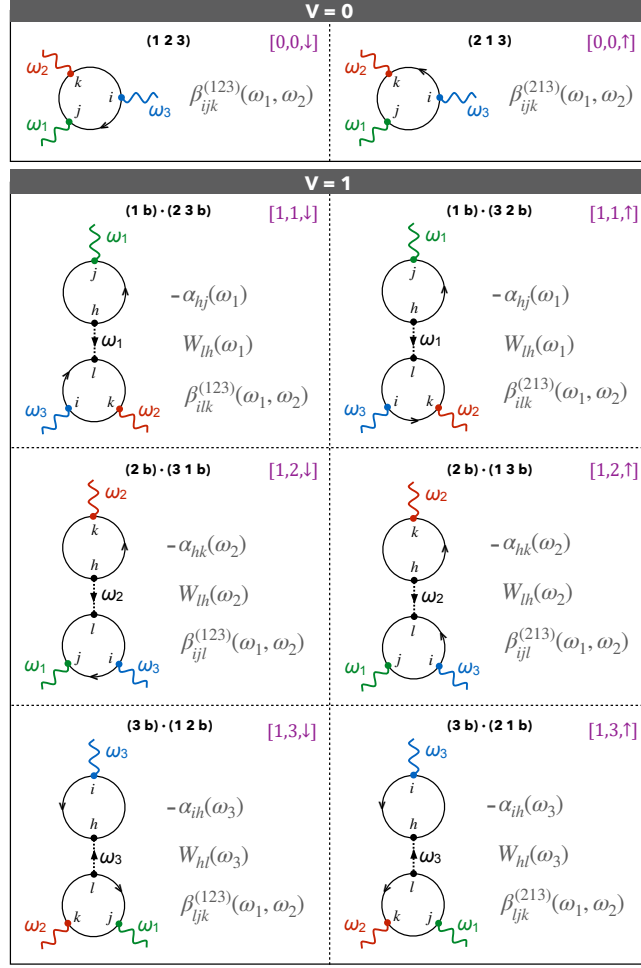


FIG. 1. List of the diagrams for bipartite systems made of a nanostructure (upper loop) and a molecule (lower loop), when $V = 0$ and $V = 1$. The arrow of each loop indicates the position of the initial state and that of each virtual boson gives the direction of the frequency (i.e. energy) exchange.

order to ease their counting and calculation, the diagrams are classified according to a nomenclature $[V, n_V, \ell_{\text{mol}}\ell_N]$. According to the value of $V \in \{1; 2; 3\}$: n_1 refers to the label of the exchanged boson frequency (e.g. ω_2 in the diagram $[1, 2, \downarrow]$ of Figure 1); n_2 refers to the label of the photon frequency interacting with the molecule (e.g. ω_1 in Figure 2); and n_3 refers to the label of the photon frequency interacting with the nanostructure loop and exactly preceding the sequence of a virtual boson and another photon (e.g. ω_1 in the diagrams (1b2bb3) of Figure 3), with $n_3 = 0$ meaning all photon frequencies (e.g. the diagrams (1b2b3b) of Figure 3). The labels ℓ_{mol} and ℓ_N correspond to the orientations of the molecule loop and the nanostructure loop, respectively: $\ell = \uparrow$ for counterclockwise direction

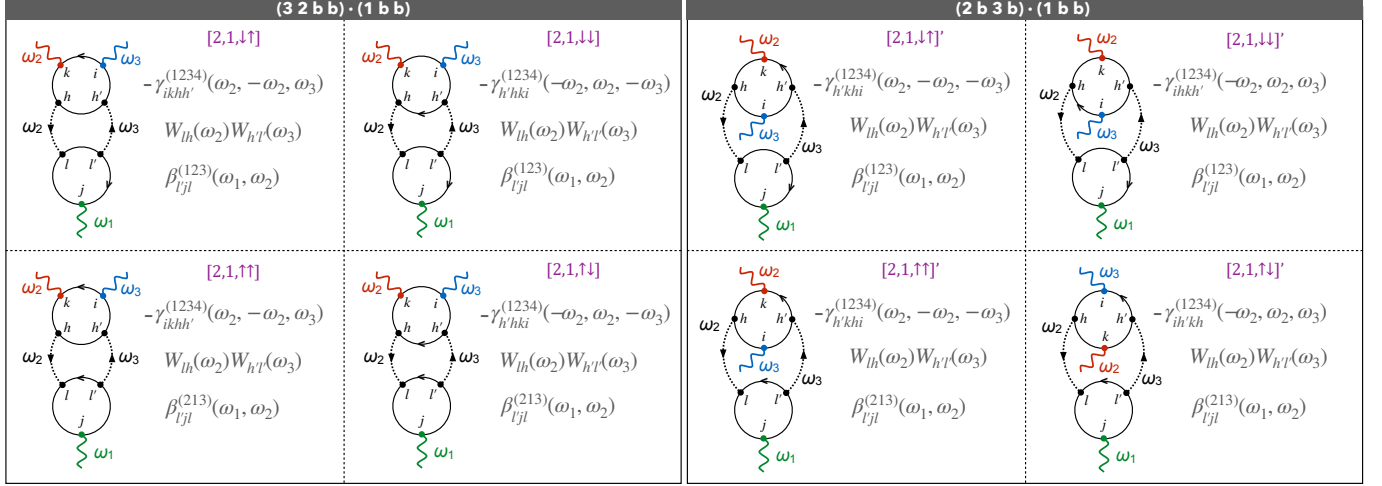


FIG. 2. List of the bipartite diagrams for $V = 2$, when the photon ω_1 is interacting with the molecule (lower loop). See Fig. 1 for the meaning of loops and arrows.

and \downarrow for clockwise. As shown in Figure 1, when $V = 1$, the nanostructure loop is symmetric and ℓ_N is not relevant. In the simple case of $V = 0$, there is a single loop associated to the molecule and no virtual boson ($n_0 = 0$). Actually, the 1-loop diagrams on Figure 1, $[0, 0, \downarrow]$ and $[0, 0, \uparrow]$, correspond to the quantities $\beta_{ijk}^{(123)}$ and $\beta_{ijk}^{(213)}$ (computed in [21], recalled in Ref. [22], section 3.2), when the molecule does not experience the influence of the nanostructure. It has been shown that the canonical hyperpolarizability $\beta_{ijk}^{[0,0]} = \beta_{ijk}^{(123)} + \beta_{ijk}^{(213)}$ comes down to the usual purely molecular β_{ijk} as deduced from the density matrix formalism [26].

Diagrams with one interaction boson. Figure 1 shows the six 2-loop diagrams made of a single virtual boson linking the nanoparticle and the molecule ($V = 1$). As shown in Ref. [22] (section 5.1), pairing the diagrams of each row (i.e. computing $\beta^{[1,n_1]} = \beta^{[1,n_1,\uparrow]} + \beta^{[1,n_1,\downarrow]}$) reconstructs $\beta^{[0,0]} = \beta^{(123)} + \beta^{(213)}$, multiplied by $-\alpha^N(\omega_{n_1}) W(\omega_{n_1})$ factors, $n_1 = \{1, 2, 3\}$, where $\alpha^N(\omega)$ is the first-order polarizability of the nanostructure. For each diagram of Figure 1, it is thus possible to calculate the expression of the corresponding β function by simply reading the diagram. Introducing matrices $\mathbf{P}(\omega) = -\alpha^N(\omega) \mathbf{W}(\omega)$ and $\mathbf{Q}(\omega) = -\mathbf{W}(\omega) \alpha^N(\omega)$, for the sum of the six diagrams:

$$\beta_{ijk}^{[1,1]}(\omega_1, \omega_2) + \beta_{ijk}^{[1,2]}(\omega_1, \omega_2) + \beta_{ijk}^{[1,3]}(\omega_1, \omega_2) = \sum_{i'j'k'} \Lambda_{ii'jj'kk'}^{(1)}(\omega_1, \omega_2) \beta_{i'j'k'}^{[0,0]}(\omega_1, \omega_2), \quad (5)$$

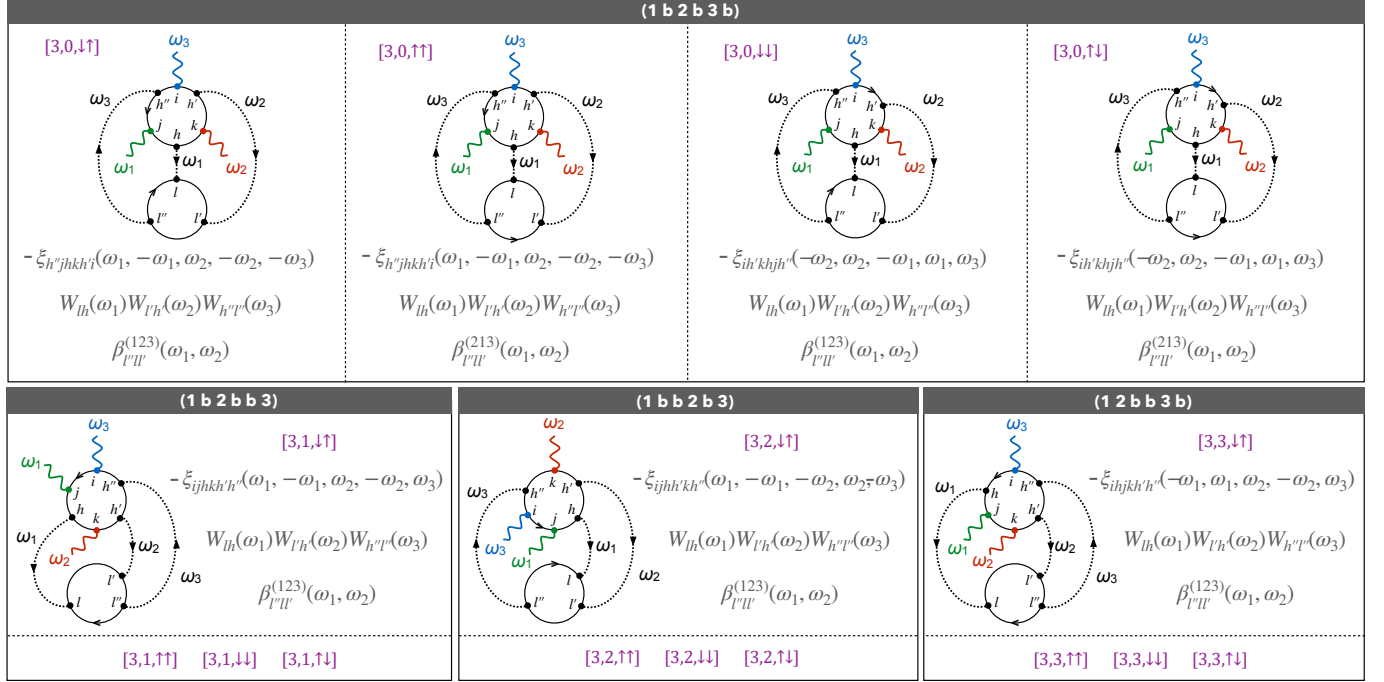


FIG. 3. List of the bipartite diagrams when $V = 3$. See Fig. 1 for the meaning of loops and arrows.

with:

$$\begin{aligned}
 \Lambda_{ii'jj'kk'}^{(1)}(\omega_1, \omega_2) = & \delta_{ii'} {}^t Q_{jj'}(\omega_1) \delta_{kk'} \\
 & + \delta_{ii'} \delta_{jj'} {}^t Q_{kk'}(\omega_2) + P_{ii'}(\omega_3) \delta_{jj'} \delta_{kk'}. \quad (6)
 \end{aligned}$$

In Eq. (5), the factor $\beta^{[0,0]}$ recalls that the SFG process is supported by the molecule, where three photons interact. Besides, Eq. (6) can be read as the superposition of three elementary interaction processes between the molecule and the nanostructure. Each of the three terms accounts for the fact that, among these three photons, only two (related to the $\delta_{xx'}$ factors) involve direct interactions between the molecule and the light beams. The third photon interacts with the nanostructure through two kinds of elementary processes: (i) as an input photon (i.e. ω_1 or ω_2), it first interacts with the nanostructure through its polarizability (factor α in Q) then propagates from the nanostructure to the molecule (factor W in Q) where it finally participates in the SFG process; (ii) as the output photon ω_3 , hence generated at the molecule, it is propagated to the nanoparticle (*via* factor W in P) where it is emitted as light (*via* factor α in P).

Diagrams with two interaction bosons. Eight of the twenty-four 2-loop diagrams made of two virtual bosons are pictured in Figure 2. The 16 other analogous diagrams are obtained

through the permutation of the three photon frequencies. Following the results of Ref. [22] (section 5.2), each column of Figure 2 (e.g. $\beta^{[2,1,\downarrow\uparrow]} + \beta^{[2,1,\uparrow\downarrow]}$) can be directly read as products of $\beta^{[0,0]}$, $W(\omega_x)W(\omega_y)$ and $-\gamma(\pm\omega_x, \pm\omega_x, \pm\omega_y)$ terms. As displayed on the figure, the four columns are associated to four γ functions whose sum can be factorized into $-b\alpha^N(\omega_x)\alpha^N(\omega_y)$ products at low temperature [21], where $b = 1/k_B T$ (Ref. [22], sections 4.1 and 5.2). The sum of the twenty-four $[2, 1, \uparrow\uparrow]$, $[2, 2, \uparrow\uparrow]$ and $[2, 3, \uparrow\uparrow]$ diagrams yields:

$$\begin{aligned} \beta_{ijk}^{[2,1]}(\omega_1, \omega_2) + \beta_{ijk}^{[2,2]}(\omega_1, \omega_2) + \beta_{ijk}^{[2,3]}(\omega_1, \omega_2) \\ = \sum_{i'j'k'} \Lambda_{ii'jj'kk'}^{(2)}(\omega_1, \omega_2) \beta_{i'j'k'}^{[0,0]}, \end{aligned} \quad (7)$$

with:

$$\begin{aligned} \Lambda_{ii'jj'kk'}^{(2)}(\omega_1, \omega_2) = P_{ii'}(\omega_3) \delta_{jj'} {}^t Q_{kk'}(\omega_2) \\ + P_{ii'}(\omega_3) {}^t Q_{jj'}(\omega_1) \delta_{kk'} + \delta_{ii'} {}^t Q_{jj'}(\omega_1) {}^t Q_{kk'}(\omega_2). \end{aligned} \quad (8)$$

Here, two of the three photons involved in the SFG process interact with the molecule through the nanostructure (the third photon directly interacts with the molecule *via* $\delta_{xx'}$), which results in a superposition of three more elementary processes.

Diagrams with three interaction bosons. Figure 3 shows the 2-loop diagrams built with three virtual bosons. Once again, the diagrams are paired to reconstruct $\beta^{[0,0]}$ (Ref. [22], section 5.3), and factorize into products of $\beta^{[0,0]}$, $W(\omega_x)W(\omega_y)W(\omega_z)$ and $-\xi(\pm\omega_x, \pm\omega_x, \pm\omega_y, \pm\omega_y, \pm\omega_z)$ terms, as displayed on Figure 3. From Ref. [22] (sections 4.2 and 5.3), grouping these ξ terms by eight leads to factorizing them into $b^2 \alpha_{ih''}^N(\omega_3) \alpha_{h'k}^N(\omega_2) \alpha_{hj}^N(\omega_1)$. Henceforth, the sum of the 16 diagrams of Figure 3 leads to:

$$\begin{aligned} \beta_{ijk}^{[3,0]}(\omega_1, \omega_2) + \beta_{ijk}^{[3,1]}(\omega_1, \omega_2) + \beta_{ijk}^{[3,2]}(\omega_1, \omega_2) + \beta_{ijk}^{[3,3]}(\omega_1, \omega_2) \\ = \sum_{i'j'k'} \Lambda_{ii'jj'kk'}^{(3)}(\omega_1, \omega_2) \beta_{i'j'k'}^{[0,0]}, \end{aligned} \quad (9)$$

with:

$$\Lambda_{ii'jj'kk'}^{(3)}(\omega_1, \omega_2) = P_{ii'}(\omega_3) {}^t Q_{jj'}(\omega_1) {}^t Q_{kk'}(\omega_2). \quad (10)$$

As expected, the single term of this last contribution represents the molecular SFG process for which the three photons interact with the nanoparticle and propagate to/from the molecule.

Direct reading of the diagrams. The previous calculations are explicitly derived in Ref. [22]. Mathematically, it requires the combination of the three sections 3, 4 and 5 of Ref. [22]. At first sight, it may seem a difficult task to compute the response functions of 48 diagrams. Fortunately, it is possible to get the complete expressions of $\Lambda_{ii'jj'kk'}^{(V)}$, Eqs. (6), (8), (10), by thoroughly reading the diagrams. Figure 4 illustrates the method in the case of $V = 2$. It starts from the diagram $[2,1,\downarrow\uparrow]$ of Figure 2 and, throughout a few steps, enables to recover the total contribution of the 24 related diagrams.

This reading procedure stems from several properties. (i) All the computed diagrams graphically connect two loops and formally combine the two associated microscopic response functions, so the response function of the system is split into the product of the response functions of each loop and the appropriate W coefficients (Figures 1, 2 and 3). (ii) The lower molecule loop is always made of 3 propagators and, as it is possible to change its orientation (from \uparrow to \downarrow according to the nomenclature), this reconstructs $\beta_{i'j'k'}^{[0,0]}$ (Ref. [22], sections 3.2 and 5). (iii) The upper nanostructure loop is made of 2, 4 or 6 propagators, giving rise to a specific class of α -, γ - or ξ -like functions. As a zero frequency is conveyed every two propagators, such functions factorize into products of $(-\alpha)$ response functions (Ref. [22], section 4), which translates into a graphical splitting of the upper loop as drawn in Figure 4. (iv) Then, the consideration of all the permutations of photon frequencies and loop orientations is known to reconstruct the full response function (Ref. [22], section 5). Figure 4(c) counts three contributions. We do not need to enumerate and draw the 24 diagrams to get them. Given the number V of virtual bosons (i.e. the number of W factors), we know that the response function $\beta_{ijk}^{[V]}$ is made of $\binom{3}{V}$ terms (as there are 3 input/output photons). For $V = 2$, we indeed count $\binom{3}{2} = 3$ terms. (v) Eventually, the assignment of the indices (i, j, k, h , etc.) is deduced from the labelling of the vertices, which is consistent over all the diagrams (i.e. identical indices correspond to identical interactions).

Total nonlinear response. In order to express the complete response function β_{ijk} of a molecule under the influence of a nanostructure, we sum all the terms $\Lambda_{ii'jj'kk'}^{(V)}$ and calculate:

$$\beta_{ijk}(\omega_1, \omega_2) = \sum_{i'j'k'} \Lambda_{ii'jj'kk'}^{(\text{total})}(\omega_1, \omega_2) \beta_{i'j'k'}^{[0,0]}(\omega_1, \omega_2), \quad (11)$$

where:

$$\begin{aligned}\Lambda_{ii'jj'kk'}^{(\text{total})}(\omega_1, \omega_2) &= \sum_{V=0}^3 \Lambda_{ii'jj'kk'}^{(V)}(\omega_1, \omega_2) \\ &= \tilde{\mathbf{L}}_{ii'}(\omega_3) \tilde{\mathbf{\Lambda}}_{jj'}(\omega_1) \tilde{\mathbf{\Lambda}}_{kk'}(\omega_2),\end{aligned}\quad (12)$$

with the matrices:

$$\tilde{\mathbf{\Lambda}}(\omega) = \mathbf{1} - \mathbf{W}(\omega) \boldsymbol{\alpha}^{\text{N}}(\omega), \quad \tilde{\mathbf{L}}(\omega) = \mathbf{1} - \boldsymbol{\alpha}^{\text{N}}(\omega) \mathbf{W}(\omega). \quad (13)$$

It sums up all molecular SFG processes for which zero, one, two or three photons interact with the nanostructure. In practical applications, molecular SFG amplification will be obtained by maximizing $\boldsymbol{\alpha}^{\text{N}}$ through resonances in the visible range. In the particular case of molecule/nanoparticle (NP) systems, this has been experimentally achieved by plasmon-enhanced [9, 27, 28] and exciton-enhanced nonlinear spectroscopies [17, 20].

III. DISCUSSION

Practical application of Eqs. (11–13) for data analysis is straightforwardly implemented in simple cases for which the polarisability is isotropic, i.e. $\boldsymbol{\alpha}^{\text{N}}(\omega) = \alpha_0(\omega)\mathbf{1}$. This is the case for quantum dots (QD), for which the value of α_0 may be found in Ref. 17, and for spherical dielectric or metallic particles in the quasistatic approximation [29]. For the latter system, the scalar polarizability matrix becomes:

$$\boldsymbol{\alpha}^{\text{NP}}(\omega) = 4\pi a^3 \varepsilon_0 \frac{\varepsilon - \varepsilon_m}{\varepsilon + 2\varepsilon_m} \mathbf{1}, \quad (14)$$

where a is the particle radius, ε the dielectric function of the sphere and ε_m the dielectric function of the surrounding medium. In the quasistatic limit, W_{lh} turns down to Eq. (4), and matrices $\tilde{\mathbf{\Lambda}}(\omega)$ and $\tilde{\mathbf{L}}(\omega)$ have simple expressions in the spherical coordinate system $(\mathbf{u}_\theta, \mathbf{u}_\phi, \mathbf{u}_R)$ linked to the nanoparticle [27, 30]:

$$\tilde{\mathbf{\Lambda}}(\omega, R) = \tilde{\mathbf{L}}(\omega, R) = \begin{pmatrix} 1 - \lambda & 0 & 0 \\ 0 & 1 - \lambda & 0 \\ 0 & 0 & 1 + 2\lambda \end{pmatrix}, \quad (15)$$

where:

$$\lambda(\omega, R) = \frac{\varepsilon - \varepsilon_m}{\varepsilon + 2\varepsilon_m} \left(\frac{a}{R}\right)^3. \quad (16)$$

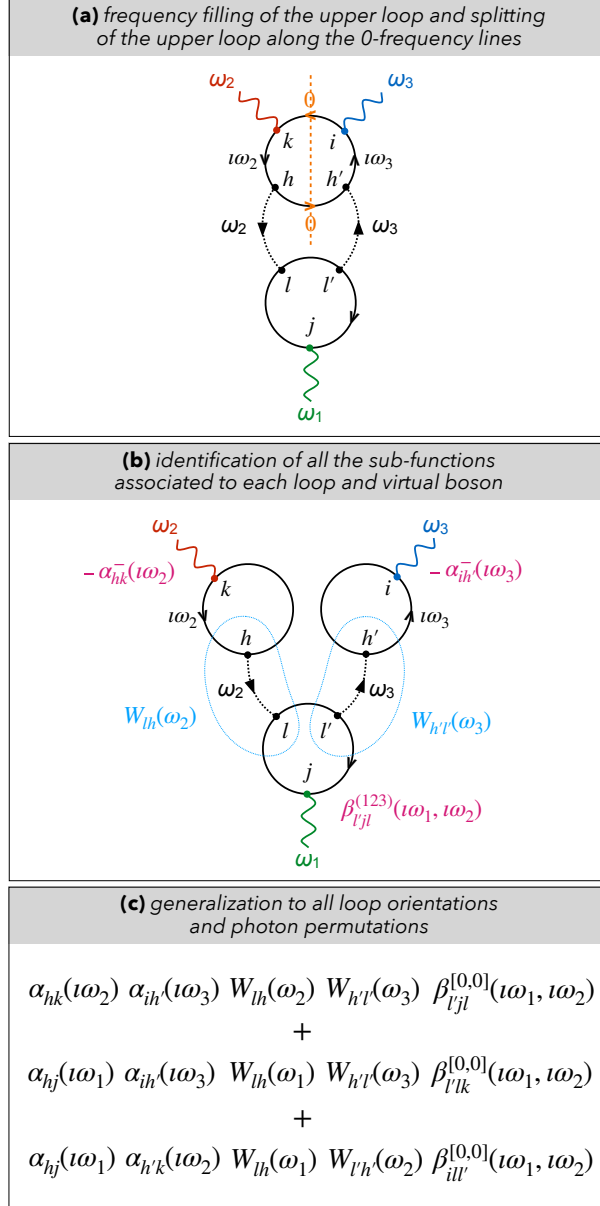


FIG. 4. Illustration of the method to directly compute the contribution of the 24 two-boson diagrams ($V = 2$) without explicit calculations, based on diagram $[2,1,\downarrow\uparrow]$ of Figure 2. The quantity α^- is the resonant part of α resulting from the upper loop splitting (see Ref. [22], section 3.1).

We recover the formula originally defined [27] as the basis change matrix between the laboratory electric field of light \mathbf{E}_0 and the molecular local electric field $\mathbf{E}_\ell = \tilde{\mathbf{\Lambda}}(\omega, \mathbf{R}) \cdot \mathbf{E}_0(\omega)$. Our diagrammatic method is thus consistent with classical calculations and gives them physical meaning by expressing $\tilde{\mathbf{\Lambda}}$ with α^{NP} and \mathbf{W} (Eq. (13)). The presence of the nanoparticle modifies the local incoming fields by creation of a dipole moment (proportional

to the far field and NP polarizability) which is then conveyed to the molecule by the dipolar Green's function \mathbf{W} . For the generated field, the nonlinear molecular dipole moment at ω_3 is first conveyed by \mathbf{W} before interacting with the particle and generating a dipolar response proportional to $\boldsymbol{\alpha}^{\text{NP}}$, hence the difference between matrices $\tilde{\mathbf{\Lambda}}$ and $\tilde{\mathbf{L}}$, which embodies the non-commutativity of the processes encoded by $\boldsymbol{\alpha}^{\text{NP}}$ and \mathbf{W} .

Our equations generalize in fact the calculation for molecules around a spherical small particle [27, 31] as they account in addition for the full $|\mathbf{R}|$ dependence of coupling matrix \mathbf{W} beyond quasistatic approximation, and for the anisotropy of the particle through the matrix form of $\boldsymbol{\alpha}$. The product of three matrix elements in Eq. (12) shows in particular that the SFG process is enhanced when the polarization of the particle becomes resonant (e.g. by excitation of the surface plasmon resonance of noble or alkali metal particles [9]).

In the context of vibrational spectroscopy, for which ω_1 is a fixed visible frequency and ω_2 a tunable IR frequency, the molecular second-order response function is usually expanded as a sum over the vibration modes $|v\rangle$, and [21]:

$$\beta_{ijk}^{[0,0]}(\omega_1, \omega_2) = \frac{1}{\hbar} \sum_v \frac{\partial_v \alpha_{ij}(\omega_3) \partial_v \mu_k}{\omega_2 - \omega_v + i\Gamma_v}. \quad (17)$$

It is now possible to write the β_{ijk} function of a molecule interacting with a nanoparticle in the form:

$$\beta_{ijk}(\omega_1, \omega_2, \mathbf{R}) = \frac{1}{\hbar} \sum_v \frac{A_{ijk}^{(v)}(\omega_1, \omega_2, \mathbf{R}_v)}{\omega_2 - \omega_v + i\Gamma_v}, \quad (18)$$

with:

$$A_{ijk}^{(v)}(\omega_1, \omega_2, \mathbf{R}_v) = \sum_{i'j'k'} \partial_v \alpha_{i'j'}(\omega_3) \partial_v \mu_{k'} \tilde{L}_{ii'}(\omega_3, \mathbf{R}_v) \times {}^t \tilde{\Lambda}_{jj'}(\omega_1, \mathbf{R}_v) {}^t \tilde{\Lambda}_{kk'}(\omega_2, \mathbf{R}_v). \quad (19)$$

The \mathbf{R}_v -dependence of \mathbf{W} must be taken into account as it corresponds to the distance, angular position and relative orientation between the nanoparticle center and the molecular group implied in the vibration mode $|v\rangle$. In terms of matrices and tensors:

$$\mathbf{A}^{(v)}(\omega_1, \omega_2, \mathbf{R}_v) = \left[\tilde{\mathbf{L}}(\omega_3, \mathbf{R}_v) \partial_v \boldsymbol{\alpha}(\omega_3) \tilde{\mathbf{\Lambda}}(\omega_1, \mathbf{R}_v) \right] \otimes \left[{}^t \tilde{\mathbf{\Lambda}}(\omega_2, \mathbf{R}_v) \partial_v \boldsymbol{\mu} \right]. \quad (20)$$

All terms in Eq. (20) have a clear meaning: $\partial_v \boldsymbol{\mu}$ measures the amplitude of the vibrational resonances whereas $\partial_v \boldsymbol{\alpha}(\omega_3)$ quantifies the molecular Raman amplitude, reconstructing the

usual amplitude of mode v in vibrational sum-frequency spectroscopy [32]. The three other terms quantify the modification of these amplitudes due to the presence of the particle, over the visible (ω_1 and ω_3) and infrared (ω_2) ranges, leading as above to potential SFG enhancements by the excitation of resonant processes.

At this stage, equation (20) can be used to compute the vibration amplitudes of SFG spectra for any bipartite nanoparticle/molecule system, on the conditions that (i) the polarizability matrix of the nanoparticle is known and (ii) a single polarizability matrix describes the whole particle (generating a nanoparticle dipole located at the origin). Condition (i) may apply to several simple systems. In addition to quantum dots and spheres, e.g. for ellipsoids, an analytic calculation may be performed: matrix α is indeed known to be scalar and diagonal along the principal axes [33]. For most particle shapes however, such an analytic calculation is not possible. Condition (ii) boils down to considering that the particle is point-like at the origin or, equivalently, that the quasi-static approximation is applied [29]. This ‘small particle’ approximation [27] is valid when $\omega|\mathbf{R}|/c \ll 1$, i.e. $2\pi|\mathbf{R}|/\lambda \ll 1$, for all characteristic distances $|\mathbf{R}|$ of the system. An upper limit of 50 nm for the particle diameter is conveniently used.

Beyond conditions (i) and (ii), for a particle of arbitrary size and shape, but also for assemblies of particles including arrays and multimers, it is still possible to calculate by numerical methods a mapping of local electric field amplitudes all around the particle as a function of the wavelength of light [34, 35] and the position \mathbf{R} of the molecule. Even if they include by construction a multipolar description of plasmonic enhancement, these methods allow reconstructing an effective $\tilde{\Lambda}(\omega, \mathbf{R})$ matrix representing the local field variations and enhancements (including tip effects [36]), from which the SFG response follows by plugging it into equations (11-12) or (18-20). These equations therefore apply to many practical situations.

The present theory leads to the evaluation, exact according to our underlying hypotheses, of the molecular hyperpolarizability of one molecule under the influence of a nearby nanoparticle. In order to evaluate the experimentally measured macroscopic nonlinear susceptibility components (i.e. several molecules interacting with a nanoparticle), individual molecular hyperpolarizabilities $\beta_{ijk}(\omega_1, \omega_2, \mathbf{R})$ are integrated over a unit surface. Integration follows the usual methods for the transposition from local ijk to laboratory frame [37], accounting for the \mathbf{R} -dependence of local β -components. When particles are used for the enhancement

of pre-deposited molecular layers, as in the SHINE-SFG geometry [28], all molecules are aligned and the \mathbf{R} -dependent integration runs over the substrate plane [27]. For molecules decorating the nanoparticle itself, angular averaging over its surface is performed, taking into account the variation of molecular orientation as a function of its position on the particle, which alters the selection rules for nonvanishing hyperpolarizability tensor components [27]. For nanorods or nanocylinders [14], the presence of the $\tilde{\mathbf{A}}(\omega, \mathbf{R})$ matrix introduces a dependence in both distance and angles. Finally, for big particles, the integration step must involve explicit phase retardation effects between molecules adsorbed on opposite sides of the particle [38, 39], which are included in the $\mathbf{W}(\omega, \mathbf{R})$ matrix in equation (3).

IV. CONCLUSION

The loop diagrammatic method and its practical implementation are general tools relevant to a variety of systems and scientific questions. Once the optical process chosen and the response function determined, drawing, selecting and calculating the appropriate diagrams is rather straightforward by following the Feynman rules [21]. Here the diagrams involved one molecular and one substrate loop (representing the nanostructure) in interaction. The latter may stand for any inorganic partner of the molecule, for example a plane substrate as in most SFG experiments, provided that the interaction hamiltonian is adapted to each case.

The formalism may extend beyond dipolar coupling to all processes involving non-radiative energy transfers in a composite system. The key parameters determining the appropriate response function lie in the interaction hamiltonians, between light and matter (\mathcal{H}_{LM}), and between subsystems (\mathcal{H}_{int}). Quadrupolar terms [40] for large particles [41] or non-spherical shapes [42], and magnetic terms for magnetic particles [43] contribute to \mathcal{H}_{int} in a multipolar development [44], as a first step towards a full Mie theory for the SFG process within nano-composite systems [45]. Symmetrically, to account for the specificities of chiral molecules [46, 47] or bulk-like surface contributions [48, 49], hyperpolarizabilities involving both magnetic and quadrupolar contributions (e.g. (eem) and (eeQ) tensors) may

be calculated by introducing the appropriate terms in \mathcal{H}_{LM} .

- [1] E. H. G. Backus, A. Eichler, A. W. Kleyn, and M. Bonn, Real-Time Observation of Molecular Motion on a Surface, *Science* **310**, 1790 (2005).
- [2] H. Arnolds, Vibrational dynamics of adsorbates – Quo vadis?, *Prog. Surf. Sci.* **86**, 1 (2011).
- [3] G. Rupprechter, A surface science approach to ambient pressure catalytic reactions, *Catal. Today* **126**, 3 (2007).
- [4] C.-S. Hsieh, R. K. Campen, M. Okuno, E. H. G. Backus, Y. Nagata, and M. Bonn, Mechanism of vibrational energy dissipation of free OH groups at the air-water interface., *Proc. Natl. Acad. Sci. U. S. A.* **110**, 18780 (2013).
- [5] R. Khatib, E. H. G. Backus, M. Bonn, M.-J. Perez-Haro, M.-P. Gaigeot, and M. Sulpizi, Water orientation and hydrogen-bond structure at the fluorite/water interface, *Scientific Reports* **6**, 24287 (2016).
- [6] D. Hu, A. Mafi, and K. C. Chou, Revisiting the Thermodynamics of Water Surfaces and the Effects of Surfactant Head Group, *J. Phys. Chem. B* **120**, 2257 (2016).
- [7] P. E. Ohno, H. f. Wang, and F. M. Geiger, Second-order spectral lineshapes from charged interfaces, *Nat. Commun.* **8**, 1032 (2017).
- [8] L. Dalstein, A. Revel, C. Humbert, and B. Busson, Nonlinear optical response of a gold surface in the visible range: A study by two-color sum-frequency generation spectroscopy. I. Experimental determination, *J. Chem. Phys.* **148**, 134701 (2018).
- [9] L. Dalstein, C. Humbert, M. Ben Haddada, S. Boujday, G. Barbillon, and B. Busson, The Prevailing Role of Hotspots in Plasmon-Enhanced Sum-Frequency Generation Spectroscopy, *J. Phys. Chem. Lett.* **10**, 7706 (2019).
- [10] N. Alyabyeva, A. Ouvrard, A.-M. Zakaria, and B. Bourguignon, Probing Nanoparticle Geometry down to Subnanometer Size: The Benefits of Vibrational Spectroscopy, *J. Phys. Chem. Lett.* **10**, 624 (2019).
- [11] P. Guyot-Sionnest, J. H. Hunt, and Y. R. Shen, Sum-frequency vibrational spectroscopy of a Langmuir film: Study of molecular orientation of a two-dimensional system, *Phys. Rev. Lett.* **59**, 1597 (1987).
- [12] Y. R. Shen, Nonlinear optical studies of surfaces, *Appl. Phys. A* **59**, 541 (1994).

- [13] A. N. Bordenyuk, C. Weeraman, A. Yatawara, H. D. Jayathilake, I. Stiopkin, Y. Liu, and A. V. Benderskii, Vibrational Sum Frequency Generation Spectroscopy of Dodecanethiol on Metal Nanoparticles, *J. Phys. Chem. C* **111**, 8925 (2007).
- [14] D. Lis, Y. Caudano, M. Henry, S. Demoustier-Champagne, E. Ferain, and F. Cecchet, Selective Plasmonic Platforms Based on Nanopillars to Enhance Vibrational Sum-Frequency Generation Spectroscopy, *Adv. Optical Mater.* **1**, 244 (2013).
- [15] L. Dalstein, M. B. Haddada, G. Barbillon, C. Humbert, A. Tadjeddine, S. Boujday, and B. Busson, Revealing the Interplay between Adsorbed Molecular Layers and Gold Nanoparticles by Linear and Nonlinear Optical Properties, *J. Phys. Chem. C* **119**, 17146 (2015).
- [16] C. Humbert, A. Dahi, L. Dalstein, B. Busson, M. Lismont, P. Colson, and L. Dreesen, Linear and nonlinear optical properties of functionalized CdSe quantum dots prepared by plasma sputtering and wet chemistry, *Journal of Colloid and Interface Science* **445**, 69 (2015).
- [17] T. Noblet, L. Dreesen, S. Boujday, C. Méthivier, B. Busson, A. Tadjeddine, and C. Humbert, Semiconductor quantum dots reveal dipolar coupling from exciton to ligand vibration, *Commun. Chem.* **1**, 76 (2018).
- [18] C. Humbert, T. Noblet, L. Dalstein, B. Busson, and G. Barbillon, Sum-Frequency Generation Spectroscopy of Plasmonic Nanomaterials: A Review, *Materials* **12**, 836 (2019).
- [19] M. Linke, M. Hille, M. Lackner, L. Schumacher, S. Schlücker, and E. Hasselbrink, Plasmonic Effects of Au Nanoparticles on the Vibrational Sum Frequency Spectrum of 4-Nitrothiophenol, *J. Phys. Chem. C* **123**, 24234 (2019).
- [20] T. Noblet, S. Boujday, C. Méthivier, M. Erard, J. Hottechamps, B. Busson, and C. Humbert, Two-Dimensional Layers of Colloidal CdTe Quantum Dots: Assembly, Optical Properties, and Vibroelectronic Coupling, *J. Phys. Chem. C* **124**, 25873 (2020).
- [21] T. Noblet, B. Busson, and C. Humbert, Diagrammatic theory of linear and nonlinear optics for composite systems, *Phys. Rev. A* **104**, 063504 (2021).
- [22] See Supplemental Material at [url] for mathematical details and theoretical foundations of the relation between Matsubara formalism and optics, the Feynman rules for computing diagrams, the definitions of (non)linear optical response functions, the procedure of factorization within diagrams, and the method to pair and sum bipartite diagrams.
- [23] A. M. Zagoskin, *Quantum theory of many-body systems: techniques and applications* (Springer, 1998).

- [24] G. D. Mahan, *Many-particle physics*, 2nd ed. (Plenum Press, 1990).
- [25] D. P. Craig and T. Thirunamachandran, *Molecular quantum electrodynamics: an introduction to radiation-molecule interaction* (Academic Press, 1984).
- [26] R. W. Boyd, *Nonlinear Optics*, 2nd ed. (Academic Press, 2003).
- [27] B. Busson and L. Dalstein, Sum-frequency spectroscopy amplified by plasmonics: The small particle case, *J. Phys. Chem. C* **123**, 26597 (2019).
- [28] Y. He, H. Ren, E.-M. You, P. M. Radjenovic, S.-G. Sun, Z.-Q. Tian, J.-F. Li, and Z. Wang, Polarization- and wavelength-dependent shell-isolated-nanoparticle-enhanced sum-frequency generation with high sensitivity, *Phys. Rev. Lett.* **125**, 047401 (2020).
- [29] C. F. Bohren and D. R. Huffman, *Absorption and scattering of light by small particles* (Wiley, 1983).
- [30] J. A. Creighton, Surface raman electromagnetic enhancement factors for molecules at the surface of small isolated metal spheres: the determination of adsorbate orientation from sers relative intensities, *Surface Science* **124**, 209 (1983).
- [31] In Ref. [27], equation (4) should be corrected: $(\tilde{\mathbf{A}}_3)_{\mu\mu'}$ should appear instead of $({}^t\tilde{\mathbf{A}}_3)_{\mu\mu'}$.
- [32] S. H. Lin and A. A. Villaeys, Theoretical description of steady-state sum-frequency generation in molecular adsorbates, *Phys. Rev. A* **50**, 5134 (1994).
- [33] C. Noguez, Surface plasmons on metal nanoparticles: The influence of shape and physical environment, *J. Phys. Chem. C* **111**, 3806 (2007).
- [34] M. A. Yurkin and A. G. Hoekstra, The discrete-dipole-approximation code adda: Capabilities and known limitations, *J. Quant. Spec. Rad. Transf.* **112**, 2234 (2011).
- [35] A. Taflove and S. Hagness, *Computational Electrodynamics: The Finite-difference Time-domain Method*, Artech House antennas and propagation library (Artech House, 2005).
- [36] R. Rodríguez-Oliveros and J. A. Sánchez-Gil, Gold nanostars as thermoplasmonic nanoparticles for optical heating, *Opt. Express* **20**, 621 (2012).
- [37] S. Roy, K.-K. Hung, U. Stege, and D. K. Hore, Rotations, Projections, Direction Cosines, and Vibrational Spectra, *Appl. Spectrosc. Rev.* **49**, 233 (2014).
- [38] S. Roke, M. Bonn, and A. V. Petukhov, Nonlinear optical scattering: The concept of effective susceptibility, *Phys. Rev. B* **70**, 115106 (2004).
- [39] H. B. de Aguiar, R. Scheu, K. C. Jena, A. G. F. de Beer, and S. Roke, Comparison of scattering and reflection sfg: a question of phase-matching, *Phys. Chem. Chem. Phys.* **14**, 6826 (2012).

- [40] A. B. Evlyukhin, C. Reinhardt, U. Zywietz, and B. N. Chichkov, Collective resonances in metal nanoparticle arrays with dipole-quadrupole interactions, *Phys. Rev. B* **85**, 245411 (2012).
- [41] N. G. Bastús, J. Piella, and V. Puntes, Quantifying the sensitivity of multipolar (dipolar, quadrupolar, and octapolar) surface plasmon resonances in silver nanoparticles: The effect of size, composition, and surface coating, *Langmuir* **32**, 290 (2016).
- [42] Q. Sun, H. Yu, K. Ueno, A. Kubo, Y. Matsuo, and H. Misawa, Dissecting the few-femtosecond dephasing time of dipole and quadrupole modes in gold nanoparticles using polarized photoemission electron microscopy, *ACS Nano* **10**, 3835 (2016).
- [43] J. Gao, H. Gu, and B. Xu, Multifunctional magnetic nanoparticles: Design, synthesis, and biomedical applications, *Acc. Chem. Res.* **42**, 1097 (2009).
- [44] R. E. Raab and O. L. de Lange, *Multipole theory in electromagnetism* (Oxford University Press, Oxford, 2005).
- [45] A. G. F. de Beer and S. Roke, Nonlinear mie theory for second-harmonic and sum-frequency scattering, *Phys. Rev. B* **79**, 155420 (2009).
- [46] S. Van Elshocht, T. Verbiest, M. Kauranen, A. Persoons, B. M. W. Langeveld-Voss, and E. W. Meijer, Direct evidence of the failure of electric-dipole approximation in second-harmonic generation from a chiral polymer film, *The Journal of Chemical Physics* **107**, 8201 (1997).
- [47] M. C. Schanne-Klein, F. Hache, A. Roy, C. Flytzanis, and C. Payraastre, Off resonance second order optical activity of isotropic layers of chiral molecules: Observation of electric and magnetic contributions, *J. Chem. Phys.* **108**, 9436 (1998).
- [48] C. Neipert, B. Space, and A. B. Roney, Generalized computational time correlation function approach: Quantifying quadrupole contributions to vibrationally resonant second-order interface-specific optical spectroscopies, *J. Phys. Chem. C* **111**, 8749 (2007).
- [49] W. Mori, L. Wang, Y. Sato, and A. Morita, Development of quadrupole susceptibility automatic calculator in sum frequency generation spectroscopy and application to methyl C—H vibrations, *J. Chem. Phys.* **153**, 174705 (2020).